SUPPLEMENT I: SOLUTION OF 1D DIFFUSION EQUATION

We consider the one-dimensional diffusion equation

$$\frac{\partial^2 c}{\partial y^2} - \frac{1}{D}\frac{\partial c}{\partial t} = 0 \tag{1}$$

with $y \in [0, L]$. As initial condition, we apply a linear gradient across the domain, $c(y, 0) = y/L$, see Fig. **S1**. At $y = 0$, the concentration is pinned to 0 to maintain a constant gradient,

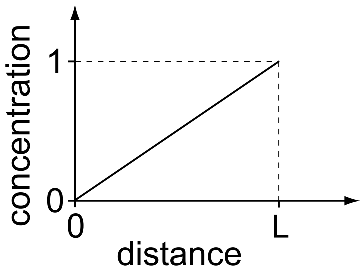

Figure S1: Initial condition $c(y, 0)$ of the concentration.

and at $y = L$, we impose a no-flux boundary condition corresponding to the side wall of the obstacle,

$$c(0, t) = 0 \qquad \text{and} \qquad \left.\frac{\partial c}{\partial y}\right|_{y=L} = 0\,. \tag{2}$$

We solve Eq. (1) by separation of variables,

$$c(y, t) = Y(y)\,T(t)\,, \tag{3}$$

which results in two separate ordinary differential equations for Y and T, respectively,

$$\frac{Y''}{Y} = k^2 \qquad \text{and} \qquad \frac{1}{D}\frac{T'}{T} = k^2\,. \tag{4}$$

They are solved by the general ansatz

$$Y(y) = A_1 e^{ky} + A_2 e^{-ky} \qquad \text{and} \qquad T(t) = C_k e^{Dk^2 t}\,. \tag{5}$$

To satisfy the boundary conditions (2), $Y(y)$ has to be a sine function with the argument $(n + \frac{1}{2})\pi y/L$, where $n = 0, 1, 2, \ldots$. This inplies $k^2 = -(n + \frac{1}{2})^2\pi^2/L^2$. The general solution is given by summing over all n,

$$c(y, t) = \sum_{n=0}^{\infty} c_n e^{-(n+\frac{1}{2})^2 \frac{\pi^2}{L^2} Dt} \sin\left[(n + \frac{1}{2})\frac{\pi y}{L}\right]\,. \tag{6}$$

The coefficients c_n have to be chosen such that the initial condition

$$c(y,0) = \sum_{n=0}^{\infty} c_n \sin\left[(n+\frac{1}{2})\frac{\pi y}{L}\right] = \frac{y}{L} \tag{7}$$

is fulfilled. The initial condition can be considered as part of a triangle wave

$$f(y) = \begin{cases} -(\frac{y}{L}+2) & : \quad y \in [-2L,-L] \\ \frac{y}{L} & : \quad y \in [-L,L] \\ 2-\frac{y}{L} & : \quad y \in [L,2L] \end{cases} \tag{8}$$

as indicated in Fig. **S2**. Developing this wave as a Fourier series yields the coefficients c_n as

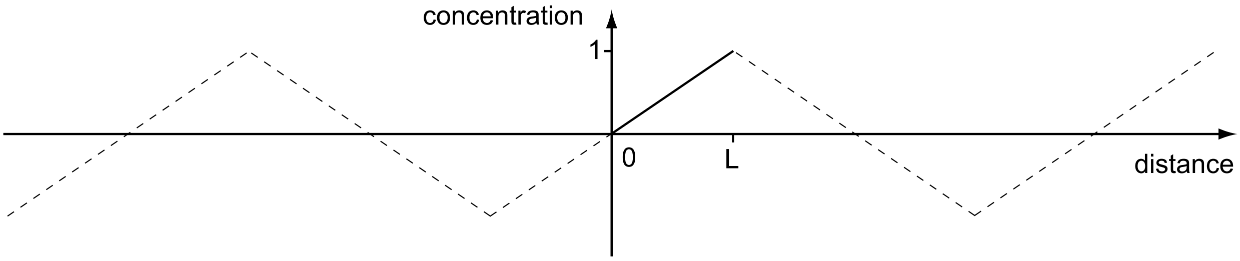

Figure S2: Initial condition $c(y,0)$ as part of a triangular wave.

outlined below. In general, every $4L$-periodic function can be developed as a Fourier series

$$f(y) = b_0 + \sum_{n=1}^{\infty}\left(a_n \sin\frac{n\pi}{2L}y + b_n \cos\frac{n\pi}{2L}y\right) . \tag{9}$$

For the function (8) the mean b_0 is zero and there are no cosine contributions. For the remaining coefficient we have

$$a_n = \frac{1}{2L}\int_{-2L}^{2L} f(y) \sin\frac{n\pi}{2L}y\,dy \tag{10}$$

$$= \frac{1}{L}\int_0^L \frac{y}{L}\sin\frac{n\pi}{2L}y\,dy + \frac{1}{L}\int_L^{2L}\left(2-\frac{y}{L}\right)\sin\frac{n\pi}{2L}y\,dy\,. \tag{11}$$

Integration by parts yields

$$a_n = \begin{cases} \frac{8}{\pi^2}\frac{(-1)^{(n-1)/2}}{n^2} & : \quad n \text{ odd} \\ 0 & : \quad n \text{ even} \end{cases} \tag{12}$$

With this, $f(y)$ can be written as

$$f(y) = \sum_{n=1}^{\infty} \frac{8}{\pi^2} \frac{(-1)^{(n-1)/2}}{n^2} \sin \frac{n\pi}{2L} y \quad \text{for } n \text{ odd} \tag{13}$$

$$= \sum_{n=0}^{\infty} \frac{8}{\pi^2} \frac{(-1)^n}{(2n+1)^2} \sin \left[(n + \frac{1}{2}) \frac{\pi y}{L} \right] \quad \text{for } n = 0, 1, 2, ... \tag{14}$$

By comparison with Eq. (7), we see that

$$c_n = \frac{8}{\pi^2} \frac{(-1)^n}{(2n+1)^2} \qquad \text{for } n = 1, 2, ... \tag{15}$$

and thus

$$c(y,t) = \frac{2}{\pi^2} \sum_{n=0}^{\infty} \frac{(-1)^n}{(n+\frac{1}{2})^2} e^{-(n+\frac{1}{2})^2 \frac{\pi^2}{L^2} Dt} \sin \left[(n + \frac{1}{2}) \frac{\pi y}{L} \right] . \tag{16}$$

SUPPLEMENT II: CONCENTRATION AT THE OBSTACLE

In Supplement I, we have shown that a one-dimensional linear gradient profile next to an impermeable obstacle evolves according to Eq. (16). At the obstacle, *i.e.* for $y = L$, Eq. (16) reduces to

$$c(L,t) = \frac{2}{\pi^2} \sum_{n=0}^{\infty} \frac{e^{-(n+\frac{1}{2})^2 \frac{\pi^2}{L^2} Dt}}{(n+\frac{1}{2})^2} \,. \tag{17}$$

We approximate this sum by the integral

$$c(L,t) = \frac{2}{\pi^2} \int_0^{\infty} \frac{e^{-(x+\frac{1}{2})^2 \frac{\pi^2}{L^2} Dt}}{(x+\frac{1}{2})^2} \, dx + \Delta \,, \tag{18}$$

where $\Delta = \frac{2}{\pi^2} \sum_{n=0}^{\infty} \Delta_n$ with

$$\Delta_n = \frac{e^{-(n+\frac{1}{2})^2 \frac{\pi^2}{L^2} Dt}}{(n+\frac{1}{2})^2} - \int_n^{n+1} \frac{e^{-(x+\frac{1}{2})^2 \frac{\pi^2}{L^2} Dt}}{(x+\frac{1}{2})^2} \, dx \,. \tag{19}$$

For Eq. (18) integration by parts yields

$$c(L,t) = \frac{4}{\pi^2} e^{-\frac{\pi^2}{4L^2} Dt} + \frac{4}{L^2} Dt \left(\int_0^{\frac{1}{2}} e^{-x^2 \frac{\pi^2}{L^2} Dt} dx - \int_0^{\infty} e^{-x^2 \frac{\pi^2}{L^2} Dt} dx \right) + \Delta \tag{20}$$

$$= \frac{4}{\pi^2} e^{-\frac{\pi^2}{4L^2} Dt} + \frac{2}{\sqrt{\pi} L} \sqrt{Dt} \left(\mathrm{erf}\left[\frac{\pi}{2L} \sqrt{Dt} \right] - 1 \right) + \Delta \,. \tag{21}$$

An analogous result is obtained for the integral in Eq. (19). An analysis of the different terms in Eq. (21) shows that the expression for $c(L,t)$ can be split into two parts that are characterized by different time scales,

$$c(L,t) = A(t) - \frac{2}{L} \sqrt{\frac{Dt}{\pi}} \,. \tag{22}$$

In Fig. **S3**, the temporal evolution of both terms is shown for typical values of D and L. The term A is equal to one and only shows a weak increase for larger times, see Fig **S3**(a). For short times, the behavior of $c(L,t)$ is dominated by the second term, note the different scales on the ordinate of Figs. **S3**(a) and (b). For small t we can thus approximate the temporal evolution of $c(L,t)$ by

$$c(L,t) \approx 1 - \frac{2}{L} \sqrt{\frac{Dt}{\pi}} \,. \tag{23}$$

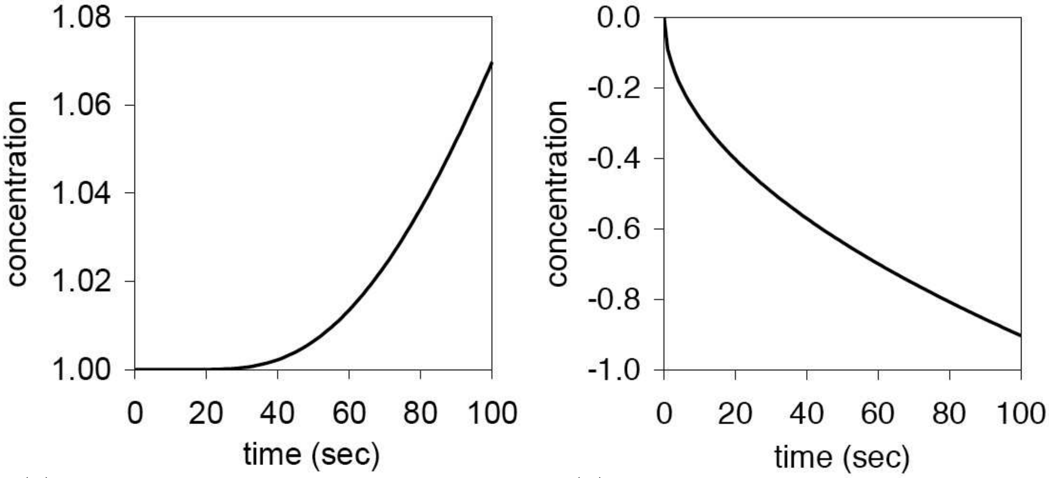

(a) (b)

Figure S3: Temporal evolution of the two terms in Eq. (22). (a) A(t) remains close to 1 and only diverges for large times. (b) At short times, the temporal evolution is dominated by the $\sqrt{t}$-dependence of the second term. For the channel half width L and the diffusion coefficient D of the chemoattractant we have chosen 250 μm and 400 μm^2/sec, respectively.

SUPPLEMENT III: ERROR ESTIMATES

1. Error in flow profile

Migration experiments in microfluidic devices are typically performed in wide channels far from the side walls to avoid boundary effects. In the numerical finite element simulations, we mimic a wide channel by assuming slip boundaries at the side walls. This corresponds to a channel of infinite width in *y*-direction. Here we analyze the error in fluid velocity that emerges from neglecting the finite extension of the channel in *y*-direction.

Between two infinitely extending slabs, the velocity profile is parabolic,

(1) $$\frac{v_s(z')}{v_0} = -6z'^2 + 1.5 \quad .$$

In a channel of rectangular cross section, on the other hand, the velocity profile is[1]

(2) $$\frac{v_{ns}(y',z')}{v_0} = \frac{1}{4}\pi^2 \frac{\sum\limits_{n\ odd}^{\infty}\sum\limits_{m\ odd}^{\infty} \frac{\cos(n\pi y')\cdot\cos(m\pi z')}{nm\left(\beta^2 n^2 + m^2\right)}}{\sum\limits_{n\ odd}^{\infty}\sum\limits_{m\ odd}^{\infty} \frac{1}{n^2 m^2\left(\beta^2 n^2 + m^2\right)}} \quad .$$

Note that we have introduced the scaling $y' = \frac{y}{L_y}$ and $z' = \frac{z}{L_z}$ with y', z' = -0.5 ... 0.5 in both cases. The velocity deviation is now defined as the difference between the real profile (2) and the approximated profile (1), $\frac{v_{ns}(y',z')}{v_0} - \frac{v_s(z')}{v_0}$.

[1] M. Spiga and G. L. Morini, A symmetric solution for velocity profile in laminar flow through rectangular ducts, *International Communications in Heat and Mass Transfer*, 1994, **21**, 469-475.

For the extension in y-direction we assume L_y = 500 μm, a typical value for microfluidic migration chambers. For the channel height values of L_z = 10, 25, and 50 μm were considered. The error in the velocity profile becomes maximal in the middle of the channel (z' = 0). Here, we find velocity deviations of 1.9 % (L_z = 10 μm), 4.9 % (L_z = 25 μm), and 10.1 % (L_z = 50 μm). An example of the velocity deviation for L_z = 25 μm is shown in Fig. S4. For the cell heights r_z in our simulations, the maximal deviation at the top of the cell never exceeds 5%.

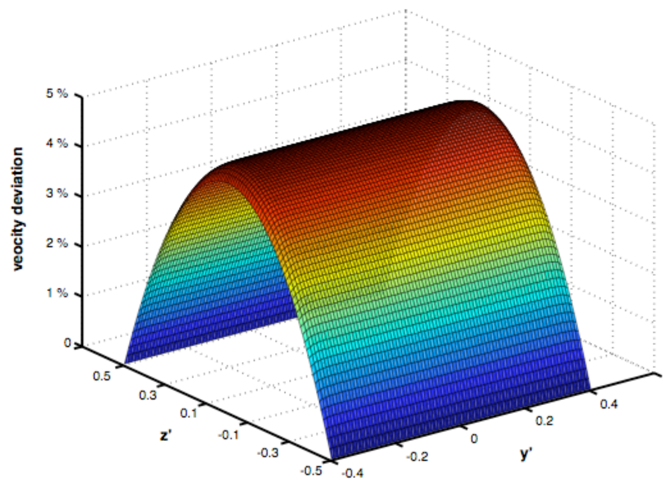

Figure S4: Error in the velocity profile for L_z = 25 μm (β = 20).

2. Error in gradient deviation

In our numerical simulations, we characterize the deviations of a concentration gradient across the cell surface from the ideal linear profile that is imposed at the inflow of the channel. Here, we analyze how the observed gradient deviation depends on the extension of the computational domain in x and y-direction. The analysis is performed for a cell with r_x = 11.25 μm and $r_y = r_z$ = 5 μm and at different flow speeds.

In Figs. S5 and S6, we show the results for a cell oriented in the direction of flow (α = 0°) and perpendicular to the flow (α = 90°), respectively. In both cases, the dependence on L_x as well as L_y is displayed. For the simulations in this paper, we chose L_x = 100 μm, L_y = 150 μm. According to the error analysis presented here, the deviation can be expected to be smaller than 0.3% in all cases.

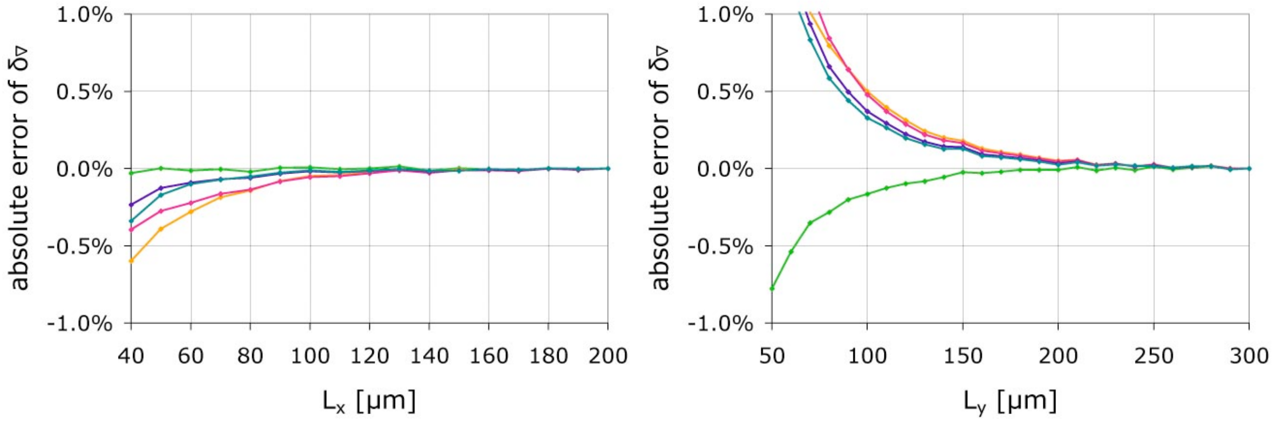

(a) (b)

Figure S5: Error in gradient deviation depending on the extension of the computational domain (a) in the direction of flow, L_x, (b) in the direction perpendicular to the flow, L_y. An elongated cell (r_x = 11.25 μm, $r_y = r_z$ = 5 μm) is considered, oriented in the direction of flow (α = 0°). The flow velocities are 0 μm/sec (green), 50 μm/sec (orange), 100 μm/sec (pink), 500 μm/sec (purple), and 1000 μm/sec (blue).

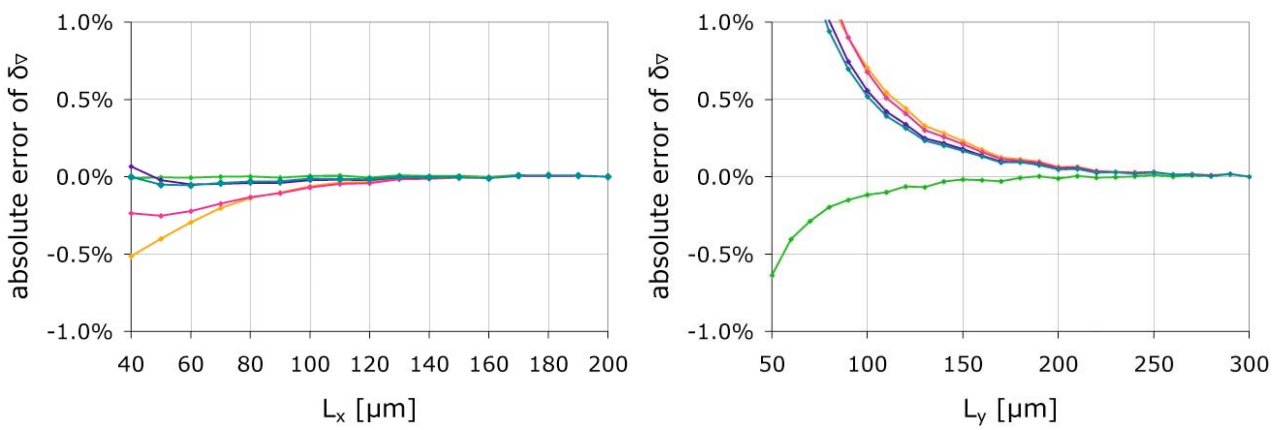

(a) (b)

Figure S6: Error in gradient deviation depending on the extension of the computational domain (a) in the direction of flow, L_x, (b) in the direction perpendicular to the flow, L_y. An elongated cell (r_x = 11.25 μm, $r_y = r_z$ = 5 μm) is considered, oriented perpendicular to the flow (α = 90°). Flow speeds as in Fig. S5.

SUPPLEMENT IV: THE INFLUENCE OF FLOW SPEED AND CHANNEL HEIGHT

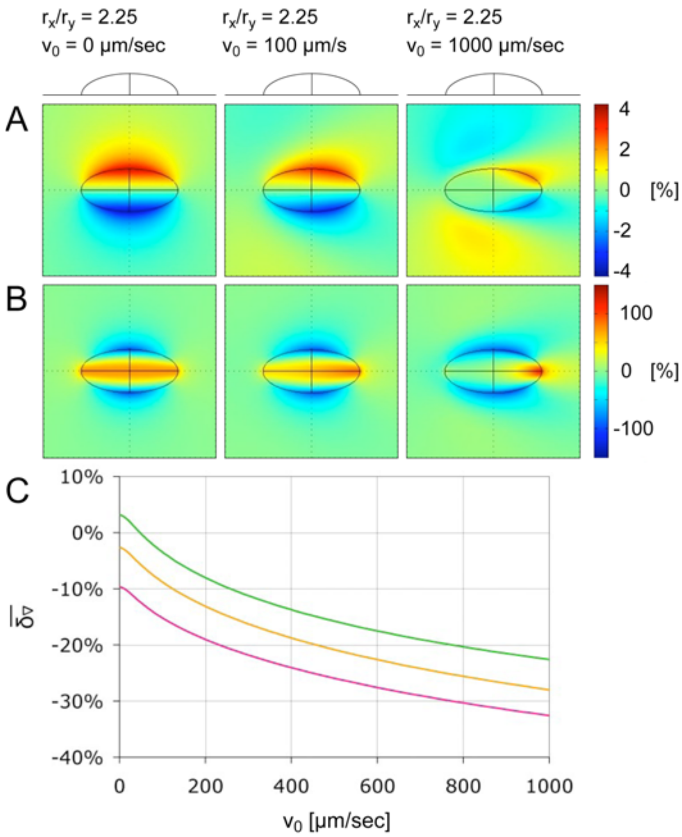

Figure S7: The effect of changing flow speed on the gradient across an elongated cell with r_z = 5 µm and α = 0° in a channel of height L_z = 25 µm; fluid flow from left to right, panel size 40 µm × 40 µm. (A) Deviation in concentration and (B) deviation in concentration gradient for a cell with r_x/r_y = 2.25. The flow speed increases from left to right, 0 µm/sec (left), 100 µm/sec (middle), 1000 µm/sec (right). (C) Global deviation in concentration gradient $\overline{\delta_\nabla}$ as a function of flow speed for three different elongations in flow direction, r_x/r_y = 1 (green) 2.25 (yellow) and 4 (pink).

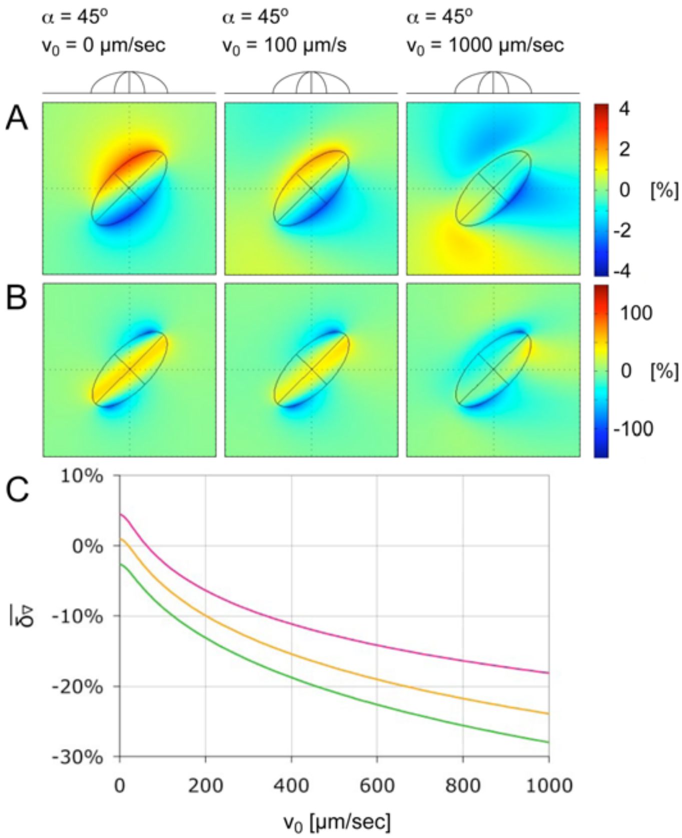

Figure S8: The effect of changing flow speed on the gradient across an elongated and rotated cell with r_x/r_y = 2.25 and r_z = 5 µm in a channel of height L_z = 25 µm; fluid flow from left to right, panel size 40 µm × 40 µm. (A) Deviation in concentration and (B) deviation in concentration gradient for an orientation of α = 45°. The flow speed increases from left to right, 0 µm/sec (left), 100 µm/sec (middle), 1000 µm/sec (right). (C) Global deviation in concentration gradient $\overline{\delta_\nabla}$ as a function of flow speed for three different orientations, 0° (green) 45° (yellow) and 90° (pink).

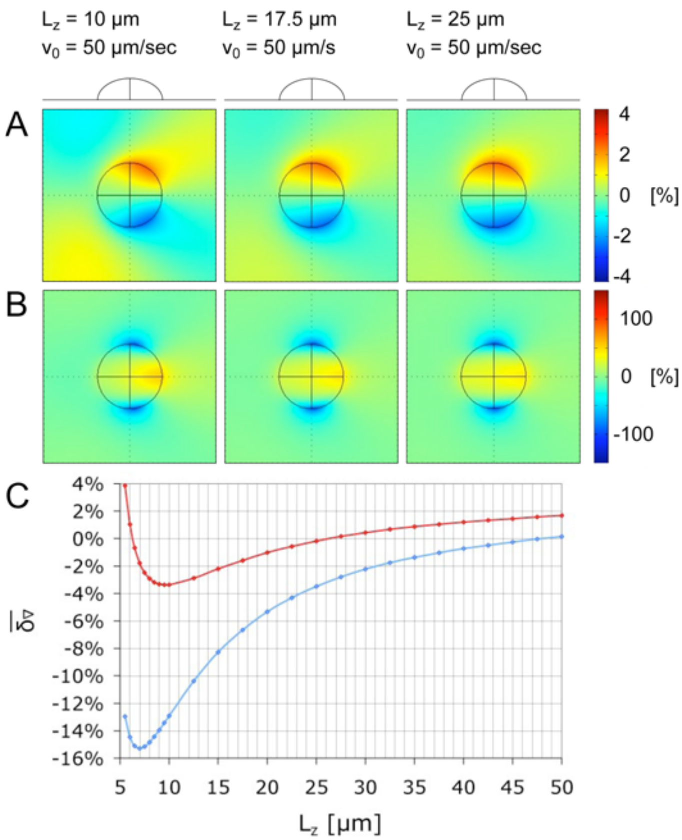

Figure S9: The effect of changing channel height L_z on the gradient across a cell of circular base with $r_x = r_y = 7.5$ µm, $r_z = 5$ µm; fluid flow from left to right, panel size 40 µm × 40 µm. (A) Deviation in concentration and (B) deviation in concentration gradient for a flow speed of 50 µm/sec. The channel height increases from left to right, $L_z = 10$ µm (left), 17.5 µm (middle), 25 µm (right). (C) Global deviation in concentration gradient $\overline{\delta_\nabla}$ as a function of channel height L_z for two different flow speeds, 50 µm/sec (red), 100 µm/sec (blue).

SUPPLEMENT V: SHEAR STRESS

It is known that many eukaryotic cells are sensitive to mechanical stimuli. Their behavior can be strongly affected by externally applied mechanical forces. In microfluidic channels, as in any other flow chamber, cells are exposed to a shear stress due to fluid flow. In the case of the chemotactic ameba *Dictyostelium discoideum*, is has been shown that shear stress can induce asymmetric intracellular localization of signaling proteins and cytoskeletal activity leading to directional locomotion (mechanotaxis) [Dalous et al., Biophys. J. 2008]. The use of microfluidic devices in chemotaxis assays and for single cell stimulation thus requires a careful control of the influence of shear stresses on cell dynamics.

We estimate the wall shear stress σ assuming a parabolic Poiseuille profile,

$$\sigma = \frac{6\eta v_0}{L_z} , \tag{1}$$

where η is the dynamic viscosity, v_0 the average fluid velocity, and L_z the channel height. In Fig. S10, we show the shear stress as a function of the average fluid velocity (A) and the channel height (B). For shear induced directional motion of *Dictyostelium* it was shown that first effects can be observed for a shear stress around σ = 0.7 Pa [Decave et al., 2003]. Most of the flow configurations considered in this work (v_0 = 50 µm/sec, L_z = 25 µm) generate shear stresses that are more than one order of magnitude below the critical value of σ = 0.7 Pa. We thus conclude, that the effects of shear stress can be neglected here. However, shear stress has to be carefully considered in cases, where the cells under investigation show a higher degree of mechanosensitivity or where the channel geometries and flow parameters are different.

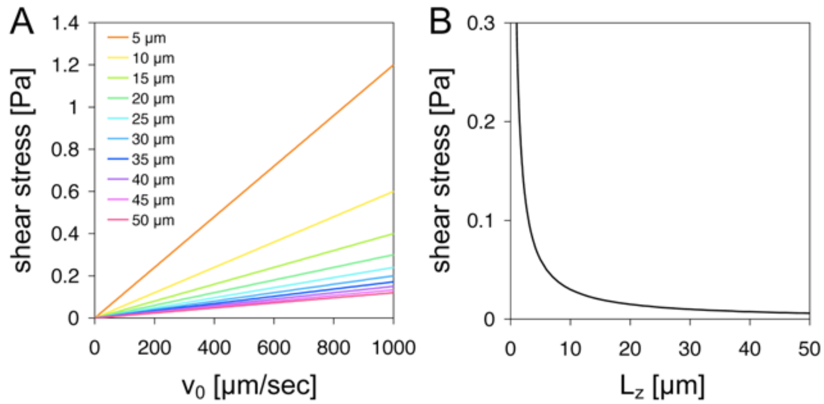

Figure S10: Wall shear stress in a microfluidic channel with aqueous flow (η = 10^{-9} kg µm^{-1} sec^{-1}). (A) Shear stress as a function of the average fluid velocity v_0 for different channel heights. (B) Shear stress as a function of channel height for an average fluid velocity of v_0 = 50 µm/sec.